Elastocapillarity and Rolling Dynamics of Solid Nanoparticles on Soft Elastic Substrates

Journal:	*Soft Matter*
Manuscript ID	SM-ART-11-2019-002280.R1
Article Type:	Paper
Date Submitted by the Author:	22-Jan-2020
Complete List of Authors:	Tian, Yuan; University of Akron, Polymer Science Liang, Heyi; University of Akron, Dobrinin, Andriy; University of Akron, Polymer Science

SCHOLARONE™
Manuscripts

Elastocapillarity and Rolling Dynamics of Solid Nanoparticles on Soft Elastic Substrates

Yuan Tian, Heyi Liang, and Andrey V. Dobrynin*

*Department of Polymer Science, University of Akron, Akron, Ohio 44325, USA*

ABSTRACT: The motion of nanoparticles on soft surfaces is the result of interplay between capillary, elastic and friction forces. To elucidate the importance of the different contributions controlling nanoparticle rolling dynamics on soft surfaces, we performed molecular dynamics simulations of solid nanoparticles in contact with soft elastic substrates. The nanoparticle motion is initiated by applying a constant force resulting in stationary, steady rolling, and accelerating states, depending on the nanoparticle-substrate work of adhesion, W, the magnitude of the net applied force, F, and the substrate shear modulus G. In the stationary state, the restoring torque produced in the contact area balances the torque due to the external force. The rolling force F_r, determining the crossover to the rolling state, is proportional to the product of the work of adhesion W and nanoparticle size R_p, $F_r \sim WR_p$. In the steady rolling state, $F > F_r$, the nanoparticle maintains a constant rolling velocity which is a manifestation of the balance between the rolling friction force and the applied force. The observed scaling relationships between the applied force and nanoparticle velocity reflect a viscoelastic nature of the substrate deformation dynamics. A nanoparticle begins to accelerate when the energy supplied to the nanoparticle exceeds the energy dissipated in the contact area due to viscoelastic substrate deformation. Using these simulation results, we have constructed a diagram of states in terms of the dimensionless parameters F/WR_p and W/GR_p.

INTRODUCTION

Elastocapillarity[1, 2] plays an important role in controlling the contact mechanics of nano- and microscale objects with elastic surfaces.[3-8] It is responsible for particle-cell [3, 5] and particle-substrate[7-13] interactions, reinforcement of interfaces between soft materials by particles [14-17] and interactions of an Atomic Force Microscopy tip with substrates of different rigidities[3, 5, 18] which is widely used to study mechanical and surface properties of soft matter and biological systems. [6, 18-20] In all these examples, the description of the equilibrium contact properties requires simultaneous consideration of capillary and elastic forces acting in the contact and vicinity of the contact area. For example, in the case of solid particles in contact with elastic substrates one has to consider changes in the substrate and particle surface free energies due to substrate deformation as the particle comes in contact with the substrate. This analysis shows that the classical Johnson, Kendall and Roberts (JKR) model[21-24] of the adhesive contact fails for soft substrates and small particles such that a more general approach accounting for elastic and capillary forces should be used to describe particle-substrate interactions. [8-11]

While the effect of elastocapillarity on static properties of contact at nano- and microscales is well understood,[8-11, 13] its role in the dynamics of contact phenomena controlling rolling and sliding friction still requires detailed examination.[25-27] These phenomena, however, are important for understanding the dynamics of self-propelled molecular machines,[28-32] particle and dust aggregation, [33-35] flow and avalanche dynamics in powders and sands,[36] the dynamics of cells and particle capture under flow conditions.[37-42] In this paper, we study the effect of elastocapillarity on rolling dynamics of solid particles moving along soft elastic surfaces. In our approach, we use a combination of coarse-grained molecular dynamics simulations to mimic the dynamics of rigid particles on elastic substrates and scaling analysis to describe general features

of rolling dynamics uncovered by simulations. In the simulations, the particle rolling motion was initiated by applying a constant external force. The motion of the particle begins with overcoming the rolling resistance in the contact area between the particle and the substrate. By changing the elastic properties of the substrate and the strength of the particle-substrate interactions, we established different rolling regimes of particle motion as a function of the applied force, particle rolling velocity, contact area, substrate shear modulus, and strength of adhesion forces. In particular, we apply scaling analysis to describe these correlations and to highlight the underlying physics controlling nanoparticle rolling dynamics.
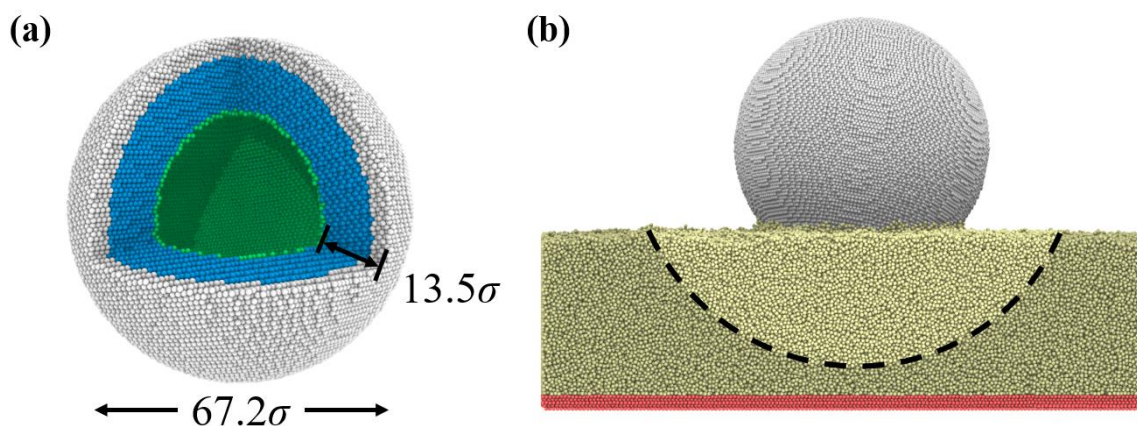

Figure 1: (a) Snapshot of the solid shell with thickness $d_0=13.5\sigma$ and outer radius $R_p=33.6\sigma$ made of regular beads (grey), rigid body beads (blue) and beads under action of the external forces (green). **(b)** Solid nanoparticle consisting of 206673 beads in contact with elastic substrate made of 972800 beads. Beads belonging to fixed bottom layer of the solid substrate made of 128000 beads are shown in red, elastic substrate beads are colored in yellow and dark yellow. The substrate beads shown in dark yellow represent "heat sink" beads that make up a dynamic group located outside of the spherical shell with a radius 60σ with respect to the center of mass of moving nanoparticle.

RESULTS AND DISCUSSION

We performed coarse-grained molecular dynamics simulations of nanoparticles in contact with elastic substrates to model nanoparticle rolling dynamics and to establish universal features of nanoparticle motion. Solid nanoparticles having 206673 beads were modeled as solid shells with thicknesses $d_0=13.5\sigma$ and radius $R_p =33.6\sigma$ (**Figure 1a**) made of Lennard-Jones (*LJ*) beads with diameter σ arranged into a hexagonal closed-packed (HCP) lattice with a lattice constant equal to σ. The inner shell of nanoparticle consisting of ten layers of 126002 beads (see layers of blue beads in **Figure 1a**) was treated as a rigid body. Nanoparticles were placed on the elastic substrates of 972800 beads made by cross-linking bead-spring chains consisting of *LJ*-beads with diameter σ and connected by the harmonic springs (see **Figure 1b**). Substrate elastic properties were controlled by changing the cross-linking density between linear chains. This allowed us to have substrates with shear moduli equal to 0.21 k_BT/σ^3 and 0.46 k_BT/σ^3 (k_B is the Boltzmann constant and T is the absolute temperature). The elastic substrate was attached to a rigid substrate consisting of 128000 beads arranged into five layers. A constant force f with the magnitude varying between 0.01 k_BT/σ and 0.26 k_BT/σ was applied to a layer of 7391 beads (see layer of green beads in **Figure 1a**) along the positive x direction. The temperature of the system during the nanoparticle motion was maintained by using the part of a substrate as a "heat sink" (see **Figure 1b**). The interaction parameters used in simulations and simulation details are discussed in the **Methods Section**.

Equilibrium Contact of Nanoparticle with Substrate. We first studied equilibrium properties of the contact between nanoparticles and elastic substrates. For solid nanoparticles in contact with an elastic substrate (**Figure 2**) having shear modulus G and work of adhesion $W = \gamma_s + \gamma_p - \gamma_{sp}$ with respect to nanoparticle (p) in contact with substrate (s) state (γ_s, γ_p, and
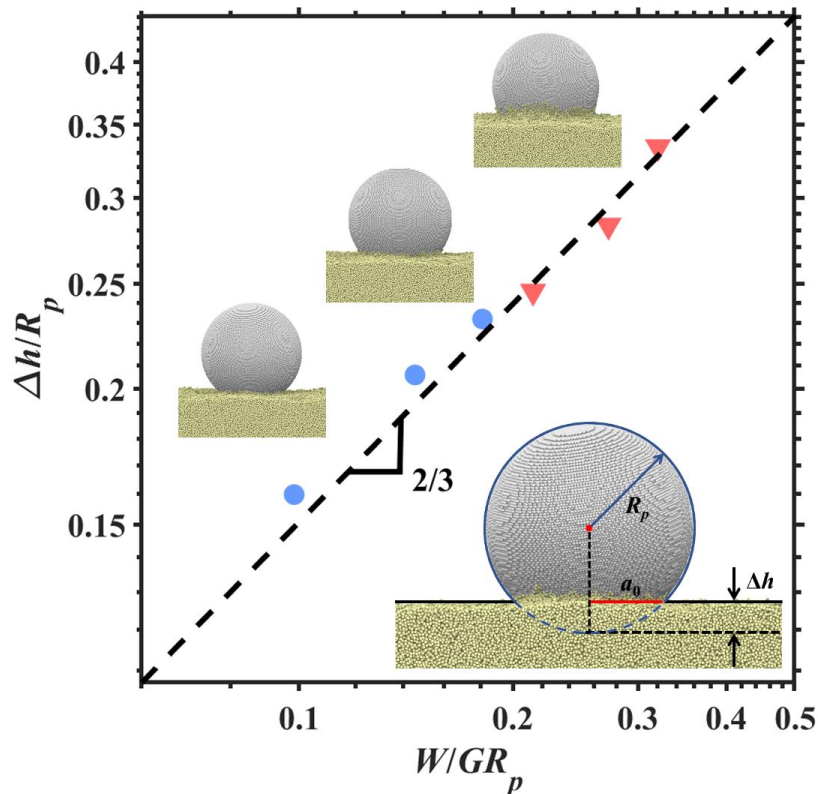
Figure 2: Dependence of the nanoparticle reduced indentation $\Delta h/R_p$ on the dimensionless parameter W/GR_p. Data corresponding to nanoparticles in contact with substrates having shear modulus $G= 0.21\ k_BT/\sigma^3$ (W=1.48 k_BT/σ^2, 1.89 k_BT/σ^2, 2.22 k_BT/σ^2) and 0.46 k_BT/σ^3 (W=1.52 k_BT/σ^2, 2.25 k_BT/σ^2, 2.80 k_BT/σ^2) are show by inverted triangles and circles respectively. Insets show typical substrate deformation and definition of the system parameters.

γ_{sp} are the surface free energies of the substrate, nanoparticle, and nanoparticle-substrate interface, respectively) the system free energy change due to indentation Δh produced by nanoparticle in the substrate has the following scaling form[43, 44]

$$\Delta F\left(\Delta h\right) \propto -WR_p\Delta h + GR_p^{1/2}\Delta h^{5/2} \tag{1}$$

The first term in eq 1 describes the surface free energy change due to nanoparticle-substrate contact while the second term accounts for the elastic energy contribution due to deformation of

the substrate produced by the nanoparticle. At equilibrium, the rate of change of the free energy

(eq 1) with indentation depth Δh is equal to zero, $\partial \Delta F (\Delta h) / \partial \Delta h = 0$, resulting in

$$\Delta h \propto R_p \left(W / GR_p \right)^{2/3} \tag{2}$$

In **Figure 2** we test the relationship (eq 2) between indentation depth and the system

macroscopic parameters. For this plot, the value of the work of adhesion W and shear modulus G

of the substrate were obtained from a separate set of simulations as described in the **Methods**
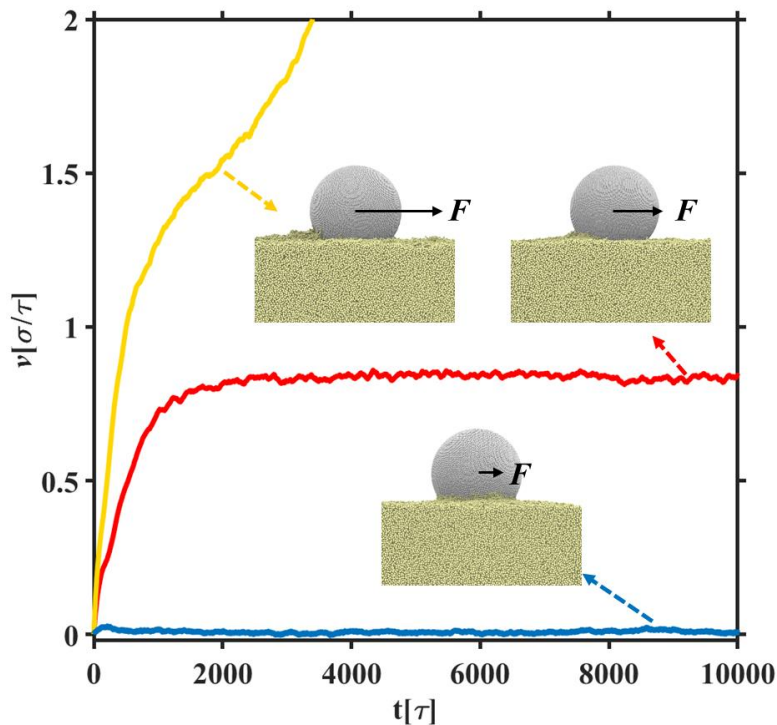
Figure 3: Dependence of the velocity of the nanoparticle center of mass during simulation

runs with the net external force F: 73.91 k_BT/σ (blue line), 665.19 k_BT/σ (red line) and

1108.65 k_BT/σ (yellow line). Nanoparticles are in contact with substrates having shear

modulus G=0.21 k_BT/σ^3 and the work of adhesion W=2.22 k_BT/σ^2. Insets illustrate evolution of

nanoparticle-substrate contact. τ is the standard Lennard-Jones time.

Section. The data follows the universal scaling dependence of the reduced indentation depth $\Delta h/R_p$ on the dimensionless ratio W/GR_p, describing the relative strength of adhesion and elastic energy contributions into the system free energy eq 1.

Rolling Dynamics of Nanoparticles. To initiate the motion of the solid nanoparticle over the substrate, we have applied a constant force f to a layer of 7391 beads as shown in **Figure 1a**. The motion of the particle started from the equilibrium state which contact properties are summarized in **Figure 2**. Under an action of the applied forces depending on the net force F, the nanoparticle could be in a stationary, steady rolling, or accelerating state as shown in **Figure 3**. As one can
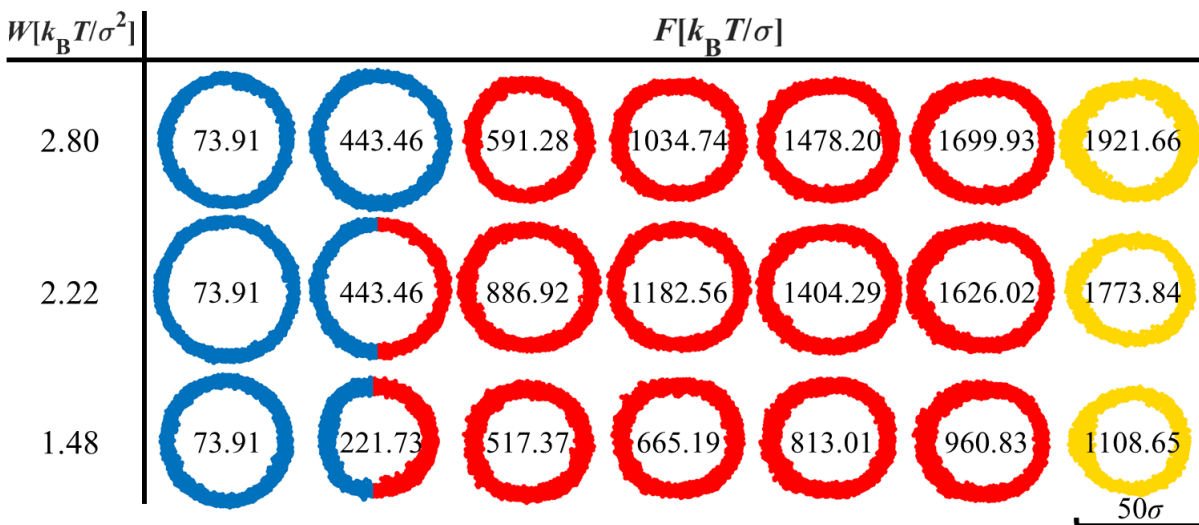
Figure 4: Evolution of the contact area as a function of the work of adhesion and magnitude of the net applied force. Numbers inside shapes correspond to the net applied force in units of k_BT/σ. Shapes colors represent different states of nanoparticle. Blue color corresponds to stationary state, red color shows contact area of nanoparticle in steady rolling stated and yellow color represents accelerating nanoparticles. Mixed color scheme corresponds to nanoparticles undergoing stick-roll motion.

see from insets in **Figure 3**, when the nanoparticle starts to move, the asymmetry of contact

between nanoparticle and substrate begins to appear. In particular, the ridge in the front edge of
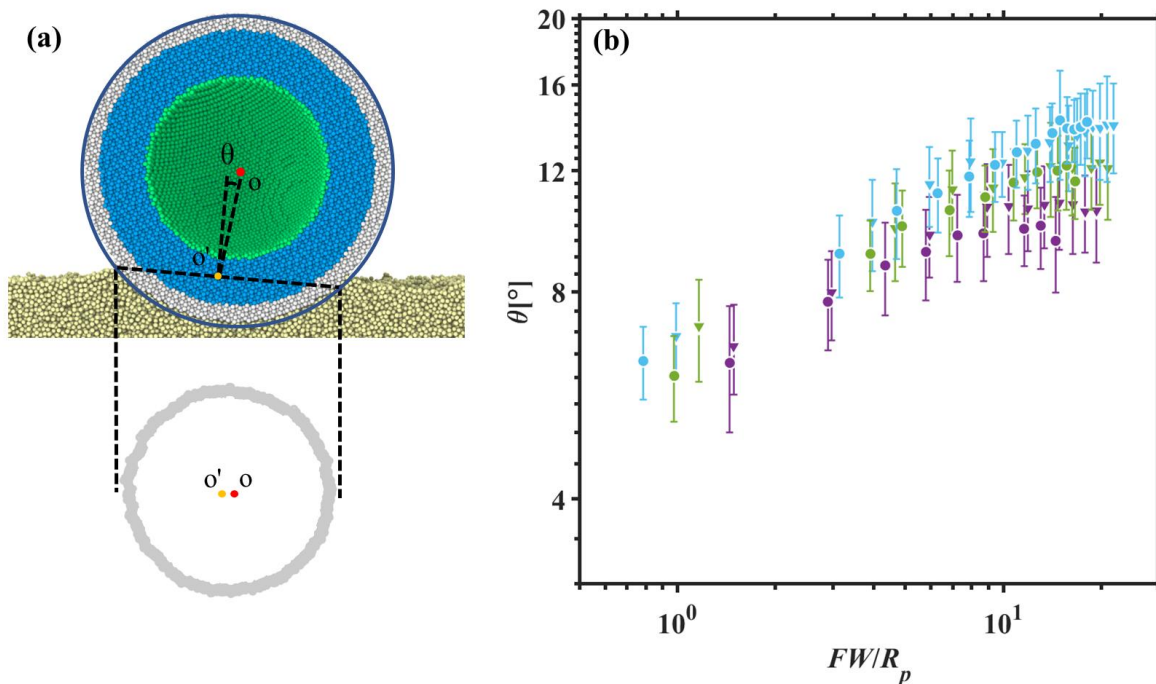
Figure 5: (a) Snapshot of nanoparticle in contact with elastic substrate showing contact area and definition of the center of mass displacement. **(b)** Dependence of the normalized displacement $\theta \approx \xi / R_p$ as a function of the reduced force F/WR_P for different values of the work of adhesion W and substrate shear modulus G: $W=1.48$ k_BT/σ^2 $G=0.21$ k_BT/σ^3 (purple inverted triangles), $W=1.89$ k_BT/σ^2 $G=0.21$ k_BT/σ^3 (green inverted triangles), $W=2.22$ k_BT/σ^2 $G=0.21$ k_BT/σ^3 (cyan inverted triangles), $W=1.52$ k_BT/σ^2 $G=0.46$ k_BT/σ^3 (purple circles), $W=2.25$ k_BT/σ^2 $G=0.46$ k_BT/σ^3 (green circles), and $W=2.80$ k_BT/σ^2 $G=0.46$ k_BT/σ^3 (cyan circles).

the nanoparticle disappears while it grows at the back edge. This contact asymmetry is quantified

in **Figure 4**, showing evolution of shape of the contact area as a function of applied force F and

work of adhesion W. Note that the crossover to rolling state happens through stick-roll motion.

Having established that the shape of the contact area of the moving nanoparticle undergoes continuous transformations with the magnitude of the applied force, we can estimate a force which is required to generate a nanoparticle's rolling motion. The nanoparticle remains at rest as long as the torque produced by applied forces is lower than that required to overcome the adhesion in the contact area. The applied torque is estimated as a net force applied to all beads forming nanoparticle F times the nanoparticle size R_p, $M_{ext} \propto FR_p$. This torque generates a deformation of the adhesive contact in such a way that the center of the cross-section area of contact is shifted by a distance ξ from the projection of the center of mass of nanoparticle on the contact plane (**Figure 5a**). This displacement results in asymmetric pressure distribution in the contact area, manifested in the appearance of the restoring torque M_r. Following results of refs[26, 45], one can estimate the restoring torque as a function of the displacement ξ as follows:

$$M_r \propto \xi Ga\Delta h \approx \xi WR_p \qquad (3)$$

In rewriting eq 3 we take into account the expression for equilibrium indentation Δh (eq 2) and for the equilibrium contact radius at small indentations, $a \propto \sqrt{R_p \Delta h}$. At equilibrium $M_{ext} = M_r$ which results in center of mass displacement $\xi \approx F/W$. **Figure 5b** combines our results for dependence of $\theta \approx \xi/R_p$ on F/WR_p. Note that WR_p is proportional to the magnitude of the critical detachment force in the JKR-model[23] of adhesive contact. It follows from this figure that the center of mass displacement is a monotonic function of the net applied force. It first increases with increasing the magnitude of the applied force, and then it begins to saturate.

In the interval of net applied forces F larger than the crossover rolling force F_r, a nanoparticle undergoes a steady rolling motion. We call this regime the *rolling regime*. We can adopt our approach developed to describe rolling motion of soft elastic shell on rigid substrates[27]

to the case of rolling dynamics of solid nanoparticles on elastic substrates. In the framework of this approach, one can show that to maintain steady rolling, the energy supplied to nanoparticle per unit time should be dissipated as viscoelastic loss in the contact area between the substrate and nanoparticle. In particular, during the rolling motion of the nanoparticle, each section of the substrate in the contact area is undergoing a time dependent deformation as the nanoparticle rolls over undeformed substrate on the right at time $t=0$ and leaves it on the left at time $t = t_{con} = 2a / v$. The compression strain produced by substrate deformation can be approximated by a sinusoidal strain function with magnitude $\varepsilon_m \approx \Delta h / a$ and frequency $\omega \approx \pi / t_{con}$

$$\varepsilon(t) \approx \varepsilon_m \sin(\omega t) \approx (\Delta h / a)\sin(\pi v t / 2a) \tag{4}$$

The average rate of energy density dissipation by substrate compression during the contact time t_{con} is estimated as

$$\dot{u}(\omega) = t_{con}^{-1} \int_0^{t_{con}} \sigma(t) d\varepsilon(t) \propto \varepsilon_m^2 \omega G''(\omega) \tag{5}$$

where $\sigma(t)$ is the time dependent stress generated by the strain $\varepsilon(t)$, with dissipative (out of phase) component estimated as $\varepsilon_m G''(\omega)\cos(\omega t)$ ($G''(\omega)$ is the frequency dependent shear loss modulus [46]). The total rate of energy dissipation in the contact zone is obtained by multiplying $\dot{u}$ by the substrate deformation volume a^3

$$\dot{U}(v) \propto a^3 \varepsilon_m^2 \omega G''(\omega) \propto \Delta h^2 v G''(v) \tag{6}$$

In the steady rolling state, the work done per unit time by moving the nanoparticle $(F - F_r)v$ with a constant velocity v is dissipated as viscoelastic loss in the substrate

$$(F - F_r)v \approx \dot{U}(v) \approx \Delta h^2 v G''(v) \tag{7}$$

This equation defines nanoparticle velocity v as a function of the net applied force. For the range of rolling speeds v such that the substrate storage modulus is frequency independent and is equal to the equilibrium shear modulus, $G'(v) \approx G$, we can use eq 2 to estimate substrate deformation Δh. Using eq 2 and taking into account that for small indentations contact radius

$$a \approx a_0 \approx \sqrt{R_p \Delta h} \approx R_p \left(W / G R_p \right)^{1/3} \tag{8}$$

we can express $\Delta h^2 \approx W a_0 / G$. Substitution of this expression into eq 7 results in

$$\left(F - F_r \right) v \approx v W a_0 G''(v) / G \approx v W a_0 \tan \delta(v) \tag{9}$$

Thus, the rate of energy dissipation is proportional to the rate of change of the contact free energy $v W a_0$ times an efficiency coefficient $\tan \delta(v) = G''(v)/G$ - the ratio of the loss and storage modulus.[46] For network-like polymeric substrates the loss modulus is a power law function $G''(\omega) = G(\omega \tau_R)^{\beta}$ where exponent $\beta = 1$ for $\omega \tau_R \ll 1$ and $\beta = 0.5$ in the frequency range $\omega \tau_R \gg 1$ (τ_R is the Rouse time of the network strands).[46] In this approximation eq 9 has the following form

$$\left(F - F_r \right) / W a_0 \approx \left(v \tau_R / a_0 \right)^{\beta} \tag{10}$$

Thus, with increasing magnitude of the applied force, the speed of nanoparticle increases as well. When the velocity of the moving nanoparticle exceeds $v > a_0 / \tau_R$, the storage modulus becomes velocity dependent and is on the order of the loss modulus such that $G''(\omega) \approx G'(\omega) \approx G(\omega \tau_R)^{0.5}$.[46] In this case, we have to explicitly take into account the dependence of contact radius, a, on the nanoparticle velocity, v. Substituting $G'(v) \approx G(v \tau_R / a)^{0.5}$ into eq 1 and rewriting it in terms of the contact radius a, we have

$$\Delta F(a,v) \propto -Wa^2 + G(v\tau_R / a)^{0.5} a^5 / R_p^2 \qquad (11)$$

The velocity dependent contact radius is obtained by balancing the elastic energy of the substrate deformation with the surface free energy change upon contact

$$a(v) \approx (v\tau_R)^{-1/5} (WR_p^2 / G)^{2/5} \approx a_0 (a_0 / v\tau_R)^{1/5} \qquad (12)$$

It follows from eq 12 that the contact radius decreases with increasing rolling velocity, $a \propto v^{-1/5}$, which results in the decrease of the rate of energy dissipation

$$\dot{U}(v) \approx vWa(v)G''(v) / G'(v) \approx v^{4/5}Wa_0 (a_0 / \tau_R)^{1/5} \qquad (13)$$

Therefore, in this regime the energy dissipation grows slower than linear with the velocity of the
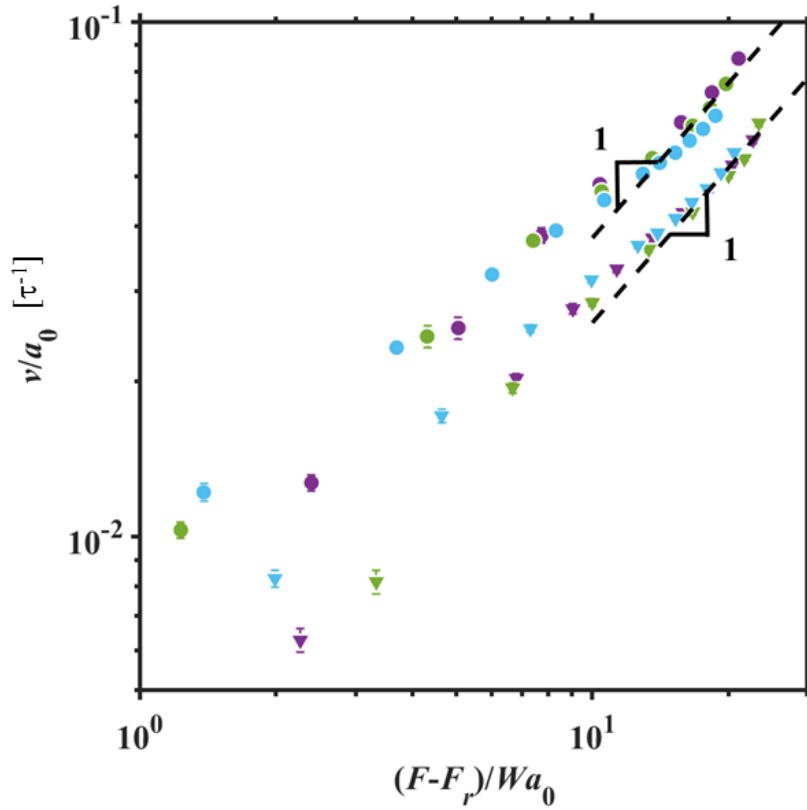

Figure 6: Universal scaling relation between normalized velocity v / a_0 and normalized net force difference $(F - F_r) / Wa_0$ (see eq 10). Symbol notations are the same as in Figure 5b.

nanoparticle. The solution of eq 7 disappears when the applied force exceeds critical value F_{acc},

$$\Delta F_{acc} v_{acc}^{1/5} \approx \Delta F_{acc} \left(a_0 / \tau_R \right)^{1/5} \approx W a_0 \left(a_0 / \tau_R \right)^{1/5} \Rightarrow \Delta F_{acc} \approx W a_0 \qquad (14)$$

where we introduced $\Delta F_{acc} = F_{acc} - F_r$. For the larger forces, $\Delta F > \Delta F_{acc}$, the nanoparticle accelerates.

Figure 6 shows the dependence of reduced nanoparticle velocity as a function of the reduced applied force (see eq 10). For this plot, we normalize nanoparticle velocity by a contact radius a_0 while the magnitude of the applied force was normalized by Wa_0. It follows from **Figure 6** that $v/a_0 \propto \left(\Delta F / Wa_0 \right)$ reflecting the fact that the loss modulus scales linear with frequency, $G''(\omega) \sim \omega$. Note that a similar regime was identified for steady rolling motion of soft shells on rigid substrates. [27]
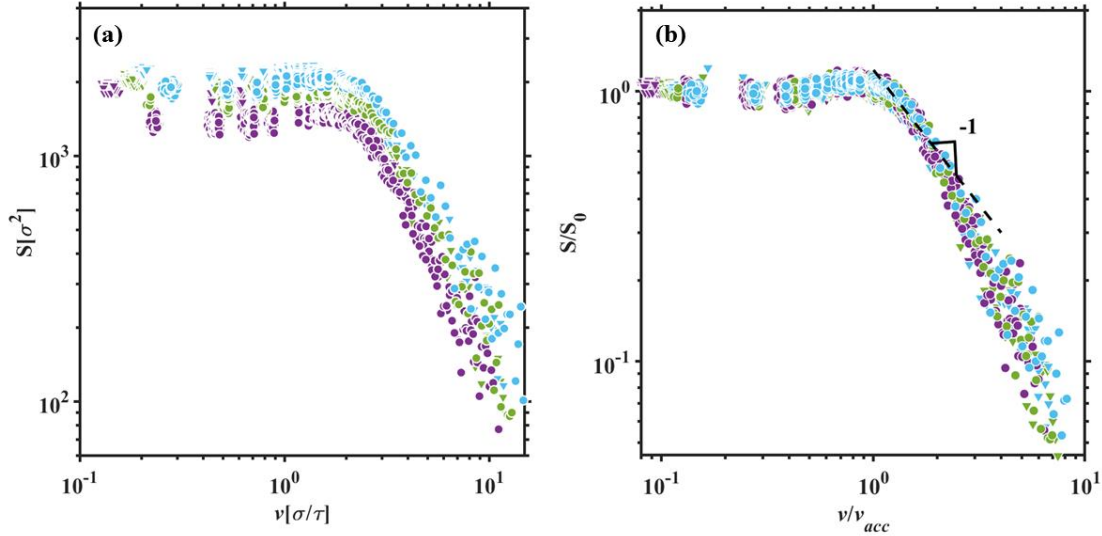
Figure 7: (a) Dependence of the instantaneous contact area S on the shell instantaneous velocity v for different values of the substrate-nanoparticle work of adhesion and substrate shear modulus. **(b)** Dependence of the normalized contact area S/S_0 on the normalized nanoparticle velocity v/v_{acc}. Symbol notations are the same as in Figure 5b.

In the steady rolling state, the contact area remains almost constant (**Figure 7a** and **Figure 4**), while in accelerating state it decreases with increasing instantaneous nanoparticle
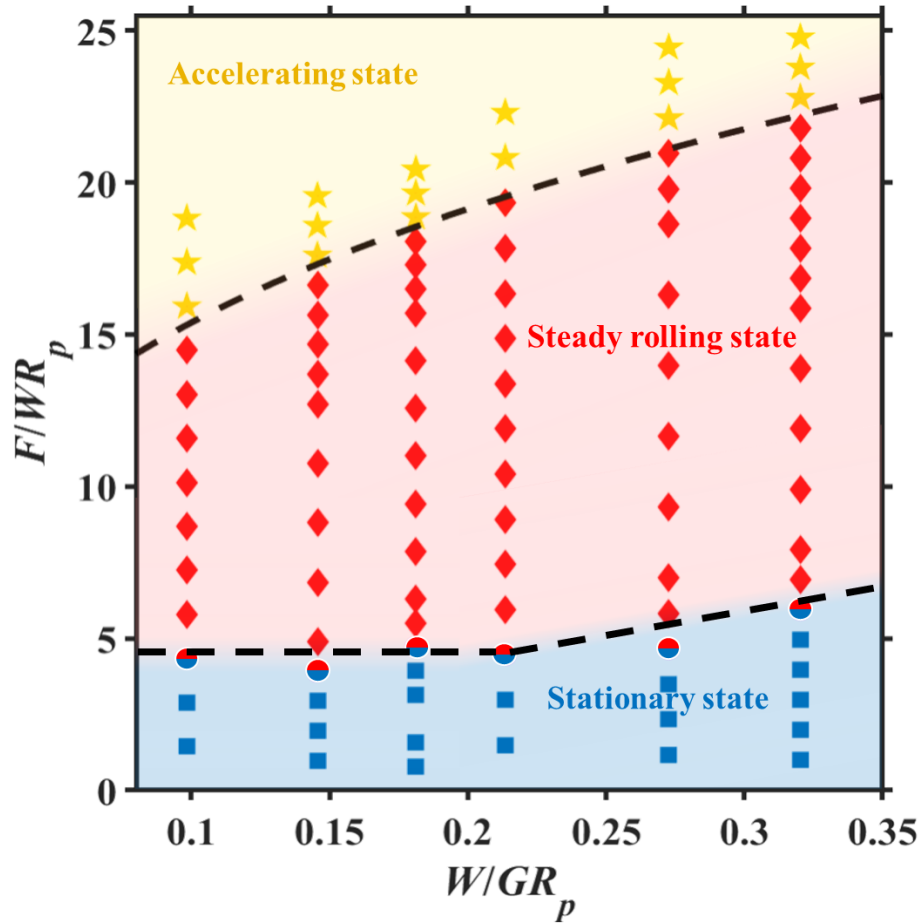
Figure 8: Diagram of states of solid nanoparticle on elastic substrates. Dashed lines show crossovers to steady rolling and accelerating regimes.

velocity v. In particular, it scales with particle velocity as $S \propto v^{-1}$. The decrease of the contact area follows from velocity dependence of the storage modulus $G'(v\tau_R/a)$ in this range of nanoparticle velocities. Note that all curves in **Figure 7a** can be collapsed by normalizing the contact area by its value in the steady rolling state S/S_0 and nanoparticle velocity by its crossover value v_{acc} into the accelerating state, v/v_{acc}, as shown in **Figure 7b**.

Analysis of the different regimes of nanoparticle motion on elastic substrates indicates that there are two dimensionless parameters that determine crossover to steady rolling state $F_r \propto WR_p$ and to accelerating state $\Delta F_{acc} \approx Wa_0 \propto WR_p \left(W / GR_p \right)^{1/3}$. Therefore, we can classify different system states by showing our data in the plane $\left(W / GR_p, F / WR_p \right)$ (**Figure 8**). This dimensionless representation of the simulation data reflects the underlying physical nature of the adhesive contact and energy dissipation during a rolling motion. In particular, the ratio W / GR_p characterizes the relative strength of capillary and elastic contributions to the system free energy, while the ratio F / WR_p gives an estimate of the force in terms of characteristic pulling force for detachment of nanoparticle from a substrate. It follows from this figure that predicted scaling dependence of the regime boundaries works for the crossover to the accelerating regime. However, the crossover normalized force to the steady rolling regime, F_r / WR_p, is constant for the interval of parameters $W / GR_p < 0.25$ while it begins to increase with W / GR_p if the opposite inequality holds.

CONCLUSIONS

We used a combination of molecular dynamics simulations and analytical calculations to show that the rolling dynamics of solid nanoparticles on elastic substrates is due to a fine interplay between adhesion and viscoelasticity in the contact zone. In particular, we demonstrated that in order to induce a nanoparticle rolling motion, the net applied force should exceed the characteristic pull-out force WR_p for adhesive contact. In the steady rolling state, the energy supplied by external force is dissipated as viscous loss in the contact zone. We have established that the nanoparticle velocity is proportional to the applied force, $v \propto \left(F - F_r \right)$. This

dependence reflects the frequency dependence of the loss modulus (eq 10 and **Figure 6**). In this

regime, the contact area between nanoparticle and substrate remains almost constant (**Figure 7a**).

However, the contact area begins to decrease with instantaneous particle velocity in the

accelerating state (**Figure 7a**). This can be explained by taking into account the velocity

dependence of the storage modulus which results in a decrease of the contact area. Scaling

analysis shows that our simulation results can be represented in universal form (**Figure 8**)

reflecting the underlying physics of the dynamics of contact phenomena. In addition, this

representation should allow comparison of simulation results with experimental studies of

nanoparticle dynamics.

The approach presented here could provide general frameworks for analysis of contact

dynamics of rolling objects such as nanoparticles and microcapsules. It is also important to point

out that our results are in agreement with recent studies of rolling dynamics of soft elastic shell

on rigid substrates. [27]

At the end we would like to comment on the limitations of our approach. Our analysis of

the nanoparticle dynamics will break down when the indentation produced by the nanoparticle in

the substrate becomes comparable with the interface thickness δ which for dense polymeric

systems is on the order of the bead size σ. In this limit the continuous approach used for

evaluation of the work of adhesion and substrate shear modulus breaks down. This takes place

when $\Delta h \leq \sigma$ or the ratio $W / GR_p \leq \left(\sigma / R_p \right)^{3/2}$. In this range of parameters one should take into

account atomistic nature of the contact and friction phenomena. [47, 48]

METHODS
Molecular dynamics simulations. A spherical nanoshell (**Figure 1a**) was made of 206673 *LJ*-

beads with diameter σ arranged into hexagonal closed-packed (HCP) lattice with a lattice

constant equal to σ. The substrate was prepared by cross-linking bead-spring chains consisting of $N = 32$ Lennard-Jones (*LJ*) beads (monomers) with diameter σ. The total number of beads in the elastic substrate was 972800. The substrate preparation and equilibration procedures have followed the approach developed in refs [9-11]. The substrate was placed on five layers of 128000 beads with each layer consisting of 160×160 beads as shown in **Figure 1b**. The system was periodic in the x and y directions.

The interactions between all beads in a system were modeled by the truncated-shifted *LJ*-potential, which for two beads separated by a distance r has the following form

$$U_{LJ}(r) = \begin{cases} 4\varepsilon_{LJ}\left[\left(\sigma/r\right)^{12} - \left(\sigma/r\right)^{6} - \left(\sigma/r_{cut}\right)^{12} + \left(\sigma/r_{cut}\right)^{6}\right] & r \le r_{cut} \\ 0 & r > r_{cut} \end{cases} \tag{15}$$

where ε_{LJ} is the *LJ*-interaction parameter and r_{cut} is the cutoff distance. The value of the cutoff distances r_{cut} and the values of the Lennard-Jones interactions parameters ε_{LJ} in terms of the thermal energy k_BT between different pairs are summarized in **Table 1**.

Table 1: Interaction Parameters

Interaction[1)	ε_{LJ} [k_BT]	r_{cut} [σ]
NP-NP	1.0	2.5
S-NP	0.8,0.9,1.0,1.2	2.5
S-S	1.0	2.5

[1) S – substrate beads, NP – beads belonging to nanoparticle.

The connectivity of beads in polymer chains, cross-linking bonds and bonds connecting beads forming a substrate were modeled by the harmonic springs described by the following potential,

$$U_{bond}(r) = \frac{1}{2}k(r-r_0)^2 \tag{16}$$

where $k = 200\ k_BT/\sigma^2$ is the spring constant and $r_0 = 0.72\sigma$ is the equilibrium bond length.

The equation of motion for the ith bead (including nanoparticle beads, and substrate beads) is

$$m\frac{\mathrm{d}\mathbf{v}_i(t)}{\mathrm{d}t} = \mathbf{F}_i(t) + f_i\mathbf{n}_x \qquad (17)$$

where m is the mass of bead which set to unity for all beads in a system, $\mathbf{v}_i(t)$ is the bead velocity, and $\mathbf{F}_i(t)$ represents the net deterministic force acting on the ith bead. The constant force f was only applied to the inner layer of 7391 beads (layer of green beads in **Figure 1a**) and was varied between 0.01 k_BT/σ and 0.26 k_BT/σ. The shell, consisting of 126002 blue beads with thickness 9σ, was treated as a rigid body shown in **Figure 1a**. To maintain a constant temperature of the system during nanoparticle motion, we applied a Langevin thermostat to the dynamic group of substrate beads outside the region with a radius of 60σ from the center of mass of the nanoparticle as shown in **Figure 1b**. This was achieved by adding the friction force, $-\xi v_i(t)\mathbf{n}_y$, and stochastic force, $F_i^R(t)\mathbf{n}_y$, terms into eq 17 describing the motion of the substrate beads outside region of radius 60σ. The stochastic force had a zero-average value $\langle F_i^R(t)\rangle = 0$ and δ-functional correlations, $\langle F_i^R(t)F_i^R(t')\rangle = 2\xi k_B T\delta_{ij}\delta(t-t')$. The friction coefficient ξ was set to $\xi = m/\tau$, where τ is the standard LJ-time $\tau = \sigma(m/\varepsilon)^{1/2}$, with ε=1.0 $k_B T$. The velocity-Verlet algorithm with a time step $\Delta t = 0.001\tau$ was used for integration of the equation of motion (eq.13). Note that in our simulations, the bottom layer of the substrate was fixed (v=0) to prevent the substrate from moving due to interaction coupling with a moving nanoparticle. In all our simulations, the temperature was set to T=1.0/k_B.

Each simulation run of nanoparticle motion started from the equilibrium state. This state was obtained by running simulations with zero external force applied to nanoparticle. The duration of each simulation run was varied to achieve the steady state or equilibrium state and could be continued up to $10^4\tau$. All simulations were performed using LAMMPS. [49]

Substrate Characterization. Substrate shear moduli at different cross-linking densities were obtained by performing simulations of the uniaxial film deformation along x-axis at constant volume. In our simulations of film deformations, the elongation ratio λ_x along the x-axis was varied from 1.00 to 1.05 with an increment $\Delta\lambda_x = 0.01$ such that the bead's coordinates were changed as $x_i \rightarrow (1+ \Delta\lambda_x)x_i$. This was done by stretching the film at a constant strain rate of 10^{-5} τ^{-1}. After deformation, all films were equilibrated for $10^4\tau$ which is followed by a production run lasting for $5 \times 10^4\tau$. The stress in the deformed films was obtained from average values of the pressure tensor in the film bulk. [50]

The work of adhesion for the substrate-nanoparticle interface was evaluated by performing simulations of the potential of mean-force calculations[51] as described in refs [9, 10, 44].

The results of this analysis are summarized in **Table 2**.

Table 2: Substrate Properties

$G[k_BT/\sigma^3]$	$\varepsilon_{LJ}\ [k_BT]^{1)}$	$\gamma_s[k_BT/\sigma^2]$	$W[k_BT/\sigma^2]$	$\Delta h[\sigma]$	$a_0[\sigma]$
	0.8	1.05	1.48	8.26	22.05
0.21	0.9	1.05	1.89	9.50	23.47
	1.0	1.05	2.22	11.22	25.08
	0.8	1.11	1.52	5.37	18.26
0.46	1.0	1.11	2.25	6.92	21.30
	1.2	1.11	2.80	7.79	22.86

AUTHOR INFORMATION
Corresponding Author
*Email: adobrynin@uakron.edu

REFERENCES

1.   De Gennes, P.-G.; Brochard-Wyart, F.; Quéré, D., *Capillarity and Wetting Phenomena: Drops, Bubbles, Pearls, Waves*. Springer: 2004.

2.   Roman, B.; Bico, J. Elasto-capillarity: deforming an elastic structure with a liquid droplet. *J. Phys. : Cond. Matt.* 22, 493101-1-16.

3.   Ebenstein, D. M.; Pruitt, L. A. Nanoindentation of biological materials. *Nano Today* **2006**, 1, 26-33.

4.   Gerberich, W. W.; Cordill, M. J. Physics of adhesion. *Reports on Progress in Physics* **2006**, 69, 2157-2203.

5.   Franz, C. M.; Puech, P. H. Atomic Force Microscopy: A Versatile Tool for Studying Cell Morphology, Adhesion and Mechanics. *Cel. Mol. Bioeng.* **2008**, 1.

6.   Harrison, A. J.; Corti, D. S.; Beaudoin, S. P. Capillary Forces in Nanoparticle Adhesion: A Review of AFM Methods. *Particul. Sci. Technol.* **2015**, 33, 1-13.

7.   Style, R. W.; Hyland, C.; Boltyanskiy, R.; Wettlaufer, J. S.; Dufresne, E. R. Surface tension and contact with soft elastic solids. *Nat. Commun.* **2013** 4, 2728.

8.   Style, R. W.; Jagota, A.; Hui, C.-Y.; Dufresne, E. R. Elastocapillarity: Surface Tension and the Mechanics of Soft Solids. *Ann. Rev. Cond. Matt.* **2016**, 8, 99-118.

9.   Cao, Z.; Stevens, M. J.; Dobrynin, A. V. Adhesion and Wetting of Nanoparticles on Soft Surfaces. *Macromolecules* **2014**, 47, 3203-3209.

10.   Cao, Z.; Stevens, M. J.; Dobrynin, A. V. Elastocapillarity: Adhesion and Wetting in Soft Polymeric Systems. *Macromolecules* **2014**, 47, 6515-6521.

11.   Carrillo, J. M. Y.; Raphael, E.; Dobrynin, A. V. Adhesion of Nanoparticles. *Langmuir* **2010**, 26, 12973-12979.

12.   Xu, X.; Jagota, A.; Hui, C.-Y. Effect of Surface Tension on the Adhesive Contact of a Rigid Sphere to a Compliant Substrate. *Soft Matter* **2014**, 10, 4625-4632.

13.   Salez, T.; Benzaquen, M.; Raphaël, É. From adhesion to wetting of a soft particle. *Soft Matter* **2013**, 9, 10699-10704.

14.   Nah, C.; Jose, J.; Ahn, J. H.; Lee, Y. S.; Gent, A. N. Adhesion of carbon black to elastomers. *Polymer Testing* **2002**, 31, 248-253.

15.   Meddahi‐Pellé, A.; Legrand, A.; Marcellan, A.; Louedec, L.; Letourneur, D.; Leibler, L. Organ repair, hemostasis, and in vivo bonding of medical devices by aqueous solutions of nanoparticles. *Angew. Chem., Int. Ed.* **2014**, 53, 6369-6373.

16.   Rose, S.; Prevoteau, A.; Elziere, P.; Hourdet, D.; Marcellan, A.; Leibler, L. Nanoparticle solutions as adhesives for gels and biological tissues. *Nature* **2014**, 505, 382.

17.   Cao, Z.; Dobrynin, A. V. Nanoparticles as adhesives for soft polymeric materials. *Macromolecules* **2016**, 49, 3586-3592.

18.   Glaubitz, M.; Medvedev, N.; Pussak, D.; Hartmann, L.; Schmidt, S.; Helm, C. A.; Delcea, M. A novel contact model for AFM indentation experiments on soft spherical cell-like particles. *Soft Matter* **2014**, 10, 6732-6741.

19.   Kuznetsova, T. G.; Starodubtseva, M. N.; Yegorenkov, N. I.; Chizhik, S. A.; Zhdanov, R. I. Atomic force microscopy probing of cell elasticity. *Micron* **2007**, 38, 824-833.

20.   Sirghi, L.; Ponti, J.; Broggi, F.; Rossi, F. Probing elasticity and adhesion of live cells by atomic force microscopy indentation. *Eur. Biophys. J.* **2008**, 935-945.

21.   Johnson, K. L.; Kendall, K.; Roberts, A. D. Surface Energy and Contact of Elastic Solids. *Proc. R. Soc. Lond. A* **1971**, 324, 301-313.

22.   Johnson, K. L. Mechanics of adhesion. *Trib. Inter.* **1998**, 31, 413-418.

23.   Johnson, K. L., *Contact Mechanics*. 9 th ed.; Cambridge University Press: 2003.

24.   Popov, V. L., *Contact Mechanics and Friction. Physical Principles and Applications*. Springer: New York, NY.

25.   Heim, L.-O.; Blum, J.; Preuss, M.; Butt, H.-J. Adhesion and Friction Forces between Spherical Micrometer-Sized Particles. *Phys. Rev. Lett.* **1999**, 83, 3328-3331.

26.   Krijt, S.; Dominik, C.; Tielens, A. G. G. M. Rolling friction of adhesive microspheres. *J. Phys. D* **2014**, 47, 175302-1-9.

27.   Tian, Y.; Liang, H.; Dobrynin, A. V. Rolling Dynamics of Nanoscale Elastic Shells Driven by Active Particles. *ACS Central Science* **2018**, 4, 1537-1544.

28.   Abendroth, J. M.; Bushuyev, O. S.; Weiss, P. S.; Barrett, C. J. Controlling Motion at the Nanoscale: Rise of the Molecular Machines. *ACS Nano* **2015**, 9, 7746-7768.

29.   Browne, W. R.; Feringa, B. L. Making molecular machines work. *Nat. Nano.* **2006**, 1, 25-35.

30.   Kolmakov, G. V.; Schaefer, A.; Aranson, I.; Balazs, A. C. Designing mechano-responsive microcapsules that undergo self-propelled motion. *Soft Matter* **2012**, 8, 180-190.

31.   Kolmakov, G. V.; Yashin, V. V.; Levitan, S. P.; Balazs, A. C. Designing self-propelled microcapsules for pick-up and delivery of microscopic cargo. *Soft Matter* **2011**, 7, 3168-3176.

32.   Patra, D.; Sengupta, S.; Duan, W. T.; Zhang, H.; Pavlick, R.; Sen, A. Intelligent, self-powered, drug delivery systems. *Nanoscale* **2013**, 5, 1273-1283.

33.   Blum, J.; Wurm, G. Experiments on Sticking, Restructuring, and Fragmentation of Preplanetary Dust Aggregates. *Icarus* **2000**, 143, 138-146.

34.   Blum, J.; Wurm, G. The Growth Mechanisms of Macroscopic Bodies in Protoplanetary Disks. *Annu. Rev. Astron. Astrophys.* **2008**, 46, 21-56.

35.   Kempf, S.; Pfalzner, S.; Henning, T. K. N-Particle-Simulations of Dust Growth. I. Growth Driven by Brownian Motion. *Icarus* **1999**, 141, 388-398.

36.   Forterre, Y.; Pouliquen, O. Physics of particulate flows: From sand avalanche to active suspensions in plants. *C. R. Physique* **2018**, 19, 271-284.

37.   Korn, C. B.; Schwarz, U. S. Dynamic states of cells adhering in shear flow: From slipping to rolling. *Phys. Rev. E* **2008**, 77.

38.   Luo, Z. Y.; Bai, B. F. State diagram for adhesion dynamics of deformable capsules under shear flow. *Soft Matter* **2016**, 12, 6918-6925.

39.   Maresov, E. A.; Kolmakov, G. V.; Yashin, V. V.; Van Vliet, K. J.; Balazs, A. C. Modeling the making and breaking of bonds as an elastic microcapsule moves over a compliant substrate. *Soft Matter* **2012**, 8, 77-85.

40.   Masoud, H.; Alexeev, A. Modeling magnetic microcapsules that crawl in microchannels. *Soft Matter* **2010**, 6, 794-799.

41.   Neubauer, M. P.; Poehlmann, M.; Fery, A. Microcapsule mechanics: From stability to function. *Adv. Coll. Inter. Sci.* **2014**, 207, 65-80.

42.   Kalasin, S.; Santore, M. M. Engineering Nanoscale Surface Features to Sustain Microparticle Rolling in Flow. *Acs Nano* **2015**, 9, 4706-4716.

43.   Ina, M.; Cao, Z.; Vatankhah-Varnoosfaderani, M.; Everhart, M. H.; Daniel, W. F. M.; Dobrynin, A. V.; Sheiko, S. S. From adhesion to wetting: Contact mechanics at the surfaces of super-soft brush-like elastomers. *ACS Macro Letters* **2017**, 6, 854-858.

44.   Tian, Y.; Ina, M.; Cao, Z.; Sheiko, S. S.; Dobrynin, A. V. How To Measure Work of Adhesion and Surface Tension of Soft Polymeric Materials. *Macromolecules* **2018**, 51, 4059-4067.

45.   Dominik, C.; Tielens, A. G. G. M. Resistance to rolling in the adhesive contact of two elastic spheres. *Phyl. Mag. A* **1995**, 72, 783-803.

46.   Rubinstein, M.; Colby, R. H., *Polymer Physics*. Oxford University Press: New York, NY, 2003.

47.   Persson, B. N. J., *Sliding Friction: Physical Principles and Applications*. 2nd ed.; Springer: New York, NY, 2000.

48.   Luan, B. Q.; Robbins, M. O. The breakdown of continuum models for mechanical contacts. *Nature* **2005**, 435, 929-932.

49.   Plimpton, S. Fast parallel algorithms for short-range molecular dynamics. *J. Comp. Phys.* **1995**, 117, 1-19.

50.   Liang, H. Y.; Cao, Z.; Wang, Z. L.; Dobrynin, A. V. Surface stress and surface tension in polymeric networks. *ACS Macro Letters* **2018**, 7, 116-121.

51.   Kumar, S.; Rosenberg, J. M.; Bouzida, D.; Swendsen, R. H.; Kollman, P. A. The weighted histogram analysis method for free‐energy calculations on biomolecules. I. The method. *J. Comput. Chem.* **1992**, 13, 1011-1021.